nanomaterials

MDPI

Article

Superlattices of Gadolinium and Bismuth Based Thallium Dichalcogenides as Potential Magnetic Topological Insulators

Alexandra Yu. Vyazovskaya [1,2,*], Evgeniy K. Petrov [1,2], Yury M. Koroteev [2,3], Mihovil Bosnar [4,5], Igor V. Silkin [1], Evgueni V. Chulkov [2,4,5] and Mikhail M. Otrokov [6,7,*]

1 Laboratory of Nanostructured Surfaces and Coatings, Tomsk State University, Tomsk 634050, Russia
2 Laboratory of Electronic and Spin Structure of Nanosystems, St. Petersburg State University, St. Petersburg 198504, Russia
3 Institute of Strength Physics and Materials Science, Tomsk 634021, Russia
4 Donostia International Physics Center (DIPC), 20018 Donostia-San Sebastián, Basque Country, Spain
5 Departamento de Polímeros y Materiales Avanzados: Física, Química y Tecnología, Facultad de Ciencias Químicas, Universidad del País Vasco UPV/EHU, 20080 Donostia-San Sebastián, Basque Country, Spain
6 Centro de Física de Materiales (CFM-MPC), Centro Mixto CSIC-UPV/EHU, 20018 Donostia-San Sebastián, Basque Country, Spain
7 IKERBASQUE, Basque Foundation for Science, 48011 Bilbao, Basque Country, Spain
* Correspondence: alex_vyaz93@mail.ru (A.Yu.V.); mikhail.otrokov@gmail.com (M.M.O.)

Abstract: Using relativistic spin-polarized density functional theory calculations we investigate magnetism, electronic structure and topology of the ternary thallium gadolinium dichalcogenides $TlGdZ_2$ (Z = Se and Te) as well as superlattices on their basis. We find $TlGdZ_2$ to have an antiferromagnetic exchange coupling both within and between the Gd layers, which leads to frustration and a complex magnetic structure. The electronic structure calculations reveal both $TlGdSe_2$ and $TlGdTe_2$ to be topologically trivial semiconductors. However, as we show further, a three-dimensional (3D) magnetic topological insulator (TI) state can potentially be achieved by constructing superlattices of the $TlGdZ_2/(TlBiZ_2)_n$ type, in which structural units of $TlGdZ_2$ are alternated with those of the isomorphic $TlBiZ_2$ compounds, known to be non-magnetic 3D TIs. Our results suggest a new approach for achieving 3D magnetic TI phases in such superlattices which is applicable to a large family of thallium rare-earth dichalcogenides and is expected to yield a fertile and tunable playground for exotic topological physics.

Keywords: density functional theory; magnetic properties; electronic structure; topological insulator

Citation: Vyazovskaya, A.Yu.; Petrov, E.K.; Koroteev, Yu.M.; Bosnar, M.; Silkin, I.V.; Chulkov, E.V.; Otrokov, M.M. Superlattices of Gadolinium and Bismuth Based Thallium Dichalcogenides as Potential Magnetic Topological Insulators. *Nanomaterials* **2023**, *13*, 38. https://doi.org/10.3390/nano13010038

Academic Editor: Zhidong Zhang

Received: 21 November 2022
Revised: 17 December 2022
Accepted: 17 December 2022
Published: 22 December 2022

1. Introduction

Magnetic topological insulators (MTIs) attract a great deal of attention nowadays [1–9] as their unique properties could find applications in dissipationless topological electronics [10], random-access memories [11], topological quantum computations [12], micro/nanoelectromechanical devices [13,14], and others. In particular, MTIs enable observation of such fundamental and practically-promising phenomena as quantum anomalous Hall [6,8,15,16] and topological magnetoelectric effects [15,17,18] (QAH and TME, respectively). Previously, transition metal elements doping [1,16] and magnetic proximity effect [19,20] approaches have been used in attempts to realize these phenomena in experiments. Although the QAHE [16,21,22] and TME [23–25] have been achieved, their observation has been limited to very low temperatures ($\leq$ 2 K) due to the inherently disordered nature of the corresponding materials [26–28].

Intrinsic MTIs and heterostructures on their basis have emerged recently as a promising alternative to observe the above-mentioned quantized topological effects at elevated temperatures [2,3,29–49]. Discovery of the first representative of the MTI class, the antiferromagnetic (AFM) TI [50] $MnBi_2Te_4$ [2,34–37], has led to an appearance of an entire family

of intrinsic MTIs, including $(MnBi_2Te_4)\cdot n(Bi_2Te_3)$ [42,44,45,51–53], $MnBi_{2-x}Sb_xTe_4$ [41,54], $(MnSb_2Te_4)\cdot n(Sb_2Te_3)$ [31,54–56], $Mn_2(Bi,Sb)_2Te_5$ [57–59], and $MnBi_2Se_4$ [31,33,60,61], which enabled significant advances. Indeed, thin $MnBi_2Te_4$ flakes have been found to show a Chern insulator state up to 30 K, achieved under an external magnetic field, but without Landau levels [5,6,62]. This has been followed by the realization of the axion insulator state [5], and eventually, of the QAHE (i.e., the QHE without external field) at 1.5 K [6], in accord with the theoretical predictions [34,35]. Very recently, the QAH regime has also been reported in the $(MnBi_2Te_4)\cdot n(Bi_2Te_3)$ heterostructures up to 6.5 K [8]. Noteworthy, apart from the $MnBi_2Te_4$-family, AFMTI state has also been predicted in some Eu-based compounds, such as $EuIn_2As_2$ [63–65].

To further consolidate the field of intrinsic MTIs, discovering new families of magnetic topologically-nontrivial systems is highly desirable. Indeed, different crystal structures and/or atomic compositions should lead to different magnetic properties, as compared to those of the $MnBi_2Te_4$-family, which should enable the realization of novel magnetic topological states of matter. In relation to a search of new MTI materials, it is instructive to observe that $Mn(Bi,Sb)_2Te_4$ and their homologous series are isostructural to those of the non-magnetic $A^{IV}(Bi,Sb)_2Te_4$, where A^{IV}= Ge, Sn, or Pb [66], which had been established to be 3D TIs before $Mn(Bi,Sb)_2Te_4$ were synthesized. Obviously, the similarity of the crystal structures and atomic compositions of the non-magnetic 3D TIs $A^{IV}(Bi,Sb)_2Te_4$ to those of (back then) topologically uncharacterized compound $MnBi_2Te_4$ hints at a likelihood of topological non-triviality of the latter, which was later confirmed both theoretically and experimentally [2,34–37]. In the present study, we will be looking for the new 3D MTI systems by choosing as a starting point yet another family of the ternary non-magnetic 3D TIs, i.e., thallium pnictogen dichalcogenides $TlXZ_2$, where X = Bi or Sb and Z = Se or Te [67–70].

$TlXZ_2$ adopt the α-$NaFeO_2$ structure (space group $R\bar{3}m$), in which the hexagonal atomic layers form the *fcc*-type stacking sequence (ABCABC) with the Tl^+ and X^{3+} cation layers separated by the Z^{2-} anion layers, –Tl–Z–X–Z–Tl–Z–X–Z–, see Figure 1a,b. In contrast to the aforementioned $Mn(Bi,Sb)_2Te_4$ or $A^{IV}(Bi,Sb)_2Te_4$ families, that are van der Waals layered materials made of septuple layer blocks, $TlXZ_2$ have no well-defined structural blocks and, thus, no van der Waals bonding, which endows the family with more 3D-like properties. Following the above-outlined logic, we may wonder if the $TlXZ_2$ family includes magnetic members and, if it does, whether they are topologically non-trivial or not. In fact, compounds with the α-$NaFeO_2$ structure and $TlXZ_2$ formula, in which the X^{3+} cation position is occupied by Gd instead of Sb or Bi, were synthesized in the powder form quite some time ago [71–74]. However, in spite of that, their magnetic and electronic properties remain poorly characterized. Indeed, on the experimental side, there only have been hints of a complex helicoidal spin arrangement in $TlGdSe_2$ [75]. On the theoretical side, the available density functional theory (DFT) studies of $TlGdZ_2$ [76] take neither spin–orbit coupling (SOC) nor Hubbard U into account, which are very important for the compounds of this family, containing both heavy elements and strongly correlated $4f$ electrons. As for a possible topologically non-trivial state in $TlGdZ_2$, which might be suspected to exist, as it does in their non-magnetic pnictogen-based $TlXZ_2$ TI counterparts, this question remains unanswered so far.

In this paper, we present a theoretical study of magnetism and electronic structure of $TlGdZ_2$ (Z = Se and Te) using relativistic spin-polarized ab initio calculations, taking the Hubbard U corrections into account. We find that for both $TlGdSe_2$ and $TlGdTe_2$ the intralayer non-collinear 120° AFM state is energetically more favorable than the FM one, indicative of the AFM coupling within Gd layers. On the other hand, the interlayer exchange coupling is found to be AFM as well, although significantly weaker, which is due to a larger Gd-Gd separation along the c axis. The electronic structure calculations including SOC reveal both $TlGdZ_2$ compounds to be topologically-trivial semiconductors with band gaps of about 1.26 and 0.56 eV for Z = Se and Te, respectively. However, we show that constructing $TlGdTe_2/(TlBiTe_2)_n$ ($n = 1, 2$) superlattices, based on the alternating –Tl–Te–

Gd–Te– and –Tl–Te–Bi–Te– units, creates a desired SOC-driven bulk band gap inversion, making these systems potential 3D MTIs both intrinsically and in the forced FM state, which can be realized under an external magnetic field. Taking into account a great variety of the $TlGdZ_2$-like compounds, selenides, tellurides and even sulfides, containing instead of Gd other rare earth (RE) elements, such as Pr, Nd, Sm, Tb, Dy, Ho, Er, and Tm [71,72,77], our study uncovers a new large family of potential magnetic topological materials of the $(TlREZ_2)_m/(TlXZ_2)_n$ type (X = Bi, Sb and Z = S, Se, Te). In these systems, by varying RE, X, Z, and m, n-parameters, it should be possible to tune not only the exchange coupling (both intra- and interlayer), but also the magnetic anisotropy and, hence, the overall spin structure. Moreover, the electronic properties such as the fundamental band gap size and character (inverted or not), $4f$ levels position, as well as the SOC strength can be varied as well. Thus, the $TlREZ_2/TlXZ_2$ superlattices are expected to provide a fertile playground for the realization of new and exotic physics. In a broader sense, our results suggest an alternative approach for achieving a 3D MTI state. Namely, apart from doping non-magnetic TIs with transition metal elements or looking for a material combining magnetism and topology intrinsically, these properties can be realized in a superlattice of the isostructural stoichiometric magnetic trivial and non-magnetic topological insulators.

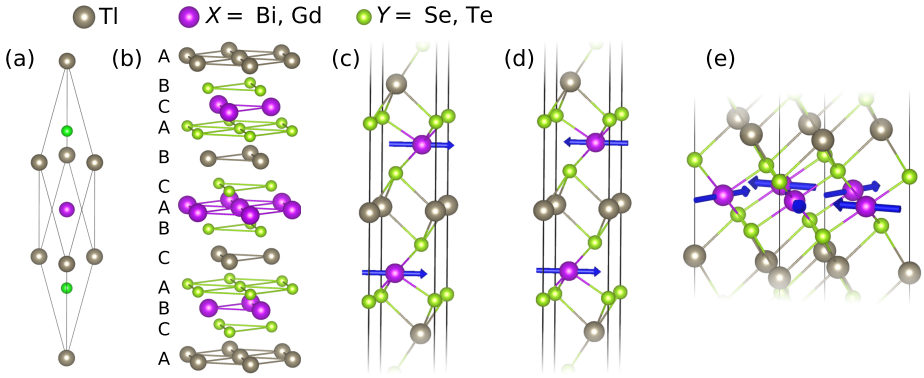

Figure 1. (**a**) Rhombohedral unit cell of $TlXZ_2$ (X = Bi, Gd, and Z = Se, Te), with grey, purple, and green balls showing Tl, X, and Z atoms, respectively. (**b**) Sketch showing the hexagonal character of the atomic layers as well as the ABCABC stacking. (**c**,**d**) Interlayer FM (**c**) and AFM (**d**) alignment of the FM Gd layers. The blue arrows show the orientations of the magnetic moments. (**e**) Intralayer non-collinear 120° AFM structure.

2. Calculation Details

The calculations were performed within the DFT using the projector augmented-wave method [78], implemented in VASP [79,80]. The generalized gradient approximation (GGA) was used to describe the exchange-correlation energy [81]. The Hamiltonian contained scalar-relativistic corrections and the SOC was taken into account by the second variation method [82]. We used the GGA + U approach [83,84] to describe the strongly localized Gd $4f$ states. The values U = 6.7 eV and J = 0.7 eV were used, typically yielding a reasonable description of the electronic structure of the Gd-containing compounds [85,86]. The electronic structures, calculated with VASP, were verified against those obtained within the full-potential linearized augmented plane wave (FLAPW) method [87] within the GGA+U approach [85,88] under the fully localized limit [89] as implemented in FLEUR [90] and a good agreement was found.

For the $TlGdZ_2$ systems, the full crystal structure optimization, i.e., that of the a and c lattice constants, c/a ratio, and atomic coordinates, was performed in the rhombohedral unit cells, while for the superlattices the hexagonal unit cells were used. The lattice parameters obtained for the bulk $TlXZ_2$ (Table 1) are in good agreement with the experimental ones [71–73,75], being slightly larger than the latter, within 1.5 %. The intralayer exchange coupling was investigated using the $(\sqrt{3} \times \sqrt{3}R30^\circ) \times 1$ hexagonal cells containing 3 atoms per layer, which is needed to model the intralayer non-collinear 120° AFM structure. To

study the interlayer exchange coupling, we used oblique cells having a hexagonal *ab* basis with the (1×1) in-plane periodicity and containing 8, 16, and 24 atoms in the cases of $TlGdZ_2$, $TlGdTe_2/(TlBiTe_2)_1$, and $TlGdTe_2/(TlBiTe_2)_2$, respectively. Atomic positions were relaxed using a force tolerance criterion of 10 meV/Å.

Table 1. Optimized hexagonal lattice constants, a and c (Å), local magnetic moment on the Gd atom, m (μ_B), total energy differences of the AFM and FM configurations inside the Gd layer ($\Delta E_{||} = E_{NCAFM} - (E_{FM} + E_{AFM})/2$, meV/[Gd pair]) and between the neighboring layers ($\Delta E_{\perp} = E_{AFM} - E_{FM}$, meV/[Gd pair]), and the bulk band gap E_g (eV).

Compound	a	c	m	$\Delta E_{\|\|}$	$\Delta E_{\perp}$	E_g
$TlGdSe_2$	4.24	23.25	7.00	−9.5	−1.3	1.26
$TlGdTe_2$	4.49	24.53	7.02	−11.7	−2.5	0.56

Surface band structures were calculated within a tight-binding approach based on the maximally localized Wannier functions [91,92] using iterative Green function method [93] implemented in WannierTools package [94].

$\mathbb{Z}_2$ topological invariant ν_0 was calculated according to [95]:

$$(-1)^{\nu_0} = \prod_{i \in \Gamma_{TRIM}} \delta_i,$$

where

$$\delta_i = \prod_{m=2,4,6...}^{N} \zeta_m(\Gamma_i).$$

$\zeta_m(\Gamma_i)$ are eigenvalues of wave function parity operator of occupied states with number m at time-reversal invariant momenta (TRIM) points Γ_{TRIM}. Calculations of $\mathbb{Z}_4$ topological invariant were carried out according to Ref. [7,96] as

$$\mathbb{Z}_4 = \sum_{i \in \Gamma_{INV}} \frac{n(\Gamma_i)^+ - n(\Gamma_i)^-}{2}.$$

where $n(\Gamma_i)^{\pm}$ is a number of occupied states with expectation values of parity ± 1 at inversion symmetry invariant momenta points Γ_i.

3. Results and Discussion

3.1. Magnetic State of $TlGdZ_2$

$TlGdZ_2$ has a markedly anisotropic crystal structure, in which the distance between Gd atoms in the basal *ab* plane is significantly smaller than that along the *c*-axis. In such quasi-2D magnets, there is a hierarchy of exchange interactions: the intralayer couplings are usually significantly stronger than the interlayer ones. We scrutinize these interactions by calculating the total energies of the following three spin configurations. In the first two, the interaction between the nearest neighbors in the Gd layers is assumed to be ferromagnetic, while their alignment along the *c*-axis can be either FM (Figure 1c) or AFM (Figure 1d), enabling evaluation of the interlayer exchange coupling. Determination of the intralayer coupling requires consideration of an additional spin structure, that could occur if the interaction between the nearest neighbors in the Gd layers was antiferromagnetic. It is well-known that in combination with a 2D hexagonal lattice, AFM exchange coupling leads to a frustration [97], typically resolving itself into a non-collinear pattern, in which three spin sublattices form an angle of 120° with respect to each other. Such a spin structure is shown in Figure 1e and will be hereinafter referred to as non-collinear antiferromagnetic (NCAFM).

While the character and strength of the interlayer exchange coupling can be conveniently characterized by $\Delta E_{\perp} = E_{AFM} - E_{FM}$, a simple difference between E_{NCAFM} and either of E_{AFM} and E_{FM} does not describe the intralayer coupling precisely. Indeed,

apart from a dominant contribution from the intralayer alignment, the total energies of the cases with FM Gd planes (i.e., E_{AFM} and E_{FM}) also include a smaller one, coming from the interlayer exchange coupling, which is either purely AFM or FM. However, in the NCAFM case, there can be no purely AFM or FM interlayer alignment. This is because of the way this spin structure combines with the ABCABC stacking of atomic layers in $TlGdZ_2$ (Figure 1b,e), leading to frustration. In detail, a Gd magnetic moment from one layer, that has three nearest magnetic neighbors in each of the two adjacent Gd layers (Figure 1b), cannot simultaneously be either AFM- or FM-coupled to all of them because we necessarily assume all of the Gd layers to be NCAFM (which is to model the intralayer AFM interaction case). Therefore, both $E_{NCAFM} - E_{FM}$ and $E_{NCAFM} - E_{AFM}$ inevitably contain a certain contribution from the coupling between layers, since it does not cancel out. Indeed, the energetical favorableness of a particular interlayer configuration (FM or AFM) makes the corresponding difference smaller and, vice versa, its unfavorableness makes it larger, which, however, has nothing to do with the intralayer coupling since E_{NCAFM} stays the same. Let us therefore account for this spurious contribution as follows: $\Delta E_{||} = E_{NCAFM} - E_{FM} + \delta = E_{NCAFM} - E_{AFM} - \delta$, where δ eliminates the contribution from the interlayer coupling. By doing simple math, we get $\Delta E_{||} = E_{NCAFM} - (E_{FM} + E_{AFM})/2$ and $\delta = -\Delta E_{\perp}/2$, δ being positive (negative) if the AFM (FM) interlayer exchange coupling is energetically favorable.

According to our total-energy calculations, $\Delta E_{||} < 0$ for both $TlGdSe_2$ and $TlGdTe_2$. In the former case, the energy gain, $|\Delta E_{||}|$, amounts to 9.5 meV per Gd pair, while in the latter it is 11.7 meV (Table 1). We thus can conclude that there is a pronounced tendency towards the non-collinear 120° AFM structure formation in the Gd layers of the $TlGdZ_2$ compounds. On the other hand, our calculations show that $\Delta E_{\perp}$ is negative, too, and equal to −1.3 (−2.5) meV per Gd pair for $TlGdSe_2$ ($TlGdTe_2$), signaling the AFM character of the interaction between neighboring Gd planes. As expected, the interlayer coupling is significantly weaker than the intralayer one, which is due to the quasi-2D magnetic character of these compounds, determined by their layered crystal structure. Indeed, the interlayer Gd-Gd distance along c is significantly larger than the in-plane one, e.g., 8.13 Å vs. 4.24 Å for $TlGdSe_2$. Still, these values cannot be considered as negligible, since $\Delta E_{\perp}$ of similar magnitude have been calculated for $MnBi_2Te_4$ and $MnSb_2Te_4$ compounds [34,45,55], that are known to be in the magnetically three-dimensional regime. The Gd local magnetic moments in both $TlGdSe_2$ and $TlGdTe_2$ are roughly equal to 7 μ_B ($S = 7/2$), in a reasonable agreement with the available experimental data [98] and DFT calculations [76].

As has been discussed above, due to the combination of the intralayer NCAFM state and the ABCABC-type stacking of atomic planes, the interlayer exchange coupling leads to magnetic frustration. To get a deeper insight into the influence of the interlayer coupling on the $TlGdZ_2$ magnetic structure, different spin alignments between the 120°-ordered planes have been considered, as is further exemplified by $TlGdTe_2$. We first note that in the NCAFM configuration considered each Gd moment has one ferromagnetically aligned nearest neighbor in each adjacent Gd layer, while the other two nearest neighbor moments are rotated by ±120° with respect to it. The presence of the FM-coupled pairs might seem energetically unfavorable since the interlayer interaction tends to align local moments antiferromagnetically because $\Delta E_{\perp} < 0$. However, if we choose an antiparallel alignment in the same pairs, the total energy stays essentially the same (within the calculation accuracy). This is because the energy decrease due to the AFM alignment is compensated by the energy increase due to the interactions with the other two nearest neighbor moments, pointing at ±60°. The sum of the latter two moments yields a vector of the same magnitude as the first one but points in the opposite direction.

Another possibility is that the interlayer configuration is helimagnetic, which is compatible with the interlayer magnetic frustration [99,100]. It would also be in line with the results of the electron paramagnetic resonance study of $TlGdSe_2$ [75], pointing towards a possible helimagnetic state. To explore this, we have considered a spin structure in which the 120° pattern of the Gd local moments rotates by an angle $\phi = 30°$ when going from

one Gd layer to another along the *c*-axis. Here, each Gd moment is perpendicular to that of one of the nearest neighbors in each adjacent Gd layer, while with respect to the other two nearest neighbor moments it deviates by 30° from the collinear FM and AFM alignments. In such a situation, no energy gain arises either, as compared to the NCAFM structure. Still, we can exclude neither a possibility of the helix angle being incommensurate with the hexagonal symmetry nor an appearance of a broken-helix magnetic order with more than one rotation angle [65]. Noteworthy, our magnetic anisotropy energy calculations show that the SOC does not favor any particular direction of the local magnetic moment, either in-plane or out-of-plane. In this situation, the role of the dipole-dipole interaction becomes crucial, which generally favors locking of the magnetic moments within the basal plane and realization of the tail-chase structure, although a canting towards the out-of-plane direction or the amplitude modulations can also occur in some cases [101–103]. It is thus evident that the exact 3D magnetic ground state structure of both $TlGdTe_2$ and $TlGdSe_2$ is very difficult to determine using the DFT calculations. The neutron diffraction measurements, which is a standard tool used to resolve magnetic structures in experiment [65,99], are desirable for $TlGdZ_2$.

3.2. Electronic Structure of $TlGdZ_2$ (Z = Se, Te)

The bulk band structures of $TlGdZ_2$ are presented in Figure 2 (the NCAFM structure, shown in Figure 1e, is assumed). It can be seen that both $TlGdSe_2$ and $TlGdTe_2$ show insulating spectra with indirect band gaps. According to the density of states calculations, the gap sizes are 1.26 eV and 0.56 eV, respectively. In both cases, the valence band maxima are formed by *p*-states of a chalcogen, while the conduction band minima are composed of the Tl *p*- and Gd *d*-states. No signature of the SOC-driven band gap inversion is observed from the analysis of the orbital composition of the states forming the band gap edges. We further confirm the absence of the inversion by direct calculations of the density of states performed at different values of the SOC constant. Thus, we can conclude that $TlGdZ_2$ (Z = Se, Te) are topologically trivial magnetic semiconductors.

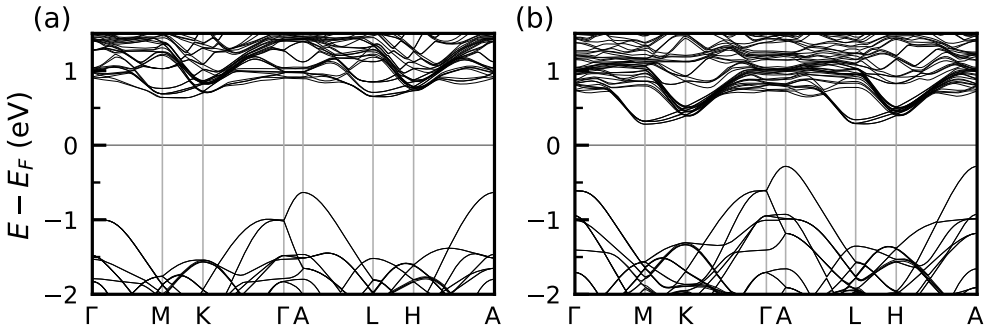

Figure 2. Bulk electronic structure of (**a**) $TlGdSe_2$ and (**b**) $TlGdTe_2$, calculated for the NCAFM spin alignment shown in Figure 1e.

3.3. $TlGdTe_2/(TlBiTe_2)_n$ Superlattices

Taking advantage of a relatively small lattice mismatch ($\Delta a \approx 2\%$) between $TlGdTe_2$ and the non-magnetic TI $TlBiTe_2$ (Supplementary Figure S1), the similarity of their atomic composition, as well as their having the same $R\bar{3}m$ crystal structure (Figure 1a), we consider bulk superlattices of the $TlGdTe_2/(TlBiTe_2)_n$ type with n =1 and 2. Their structure, shown in Figure 3a,d, comprises four-layer –Tl–Te–Gd–Te– units alternated with single (n = 1) or double (n = 2) four-layer unit of –Tl–Te–Bi–Te–. We have chosen $TlGdTe_2$ as opposed to $TlGdSe_2$ since the former has a smaller bulk band gap, which should be more easily inverted due to the strong SOC of Bi thus potentially allowing the realization of a topologically non-trivial magnetic insulating system.

After a full structural optimization (see lattice parameters in Table 2), the magnetism of $TlGdTe_2/(TlBiTe_2)_n$ has been studied. On the one hand, we find that the intralayer

NCAFM structure is by about 11.5 meV more favorable than the FM one for both $n = 1$ and $n = 2$, similar to pure $TlGdTe_2$. On the other hand, the interlayer exchange coupling for $n = 1$ weakens by an order of magnitude as compared to the latter ($\Delta E_\perp = -0.19$ meV [Table 2)] vs. -2.5 meV [Table 1)]), which is due to the increase of the Gd-Gd interlayer distance. When going from $n = 1$ to $n = 2$ it weakens by another order of magnitude.

Table 2. The same as Table 1, but for $TlGdTe_2/(TlBiTe_2)_n$. Note that for $n = 1$, the c parameter is approximately twice as large as the one for $n = 2$ because the hexagonal unit cell of the former contains 24 atoms as compared to 12 of the latter.

Superlattice	a	c	$\Delta E_{\|\|}$	$\Delta E_\perp$	E_g
$TlGdTe_2/(TlBiTe_2)_1$	4.54	48.46	-11.8	-0.19	0.086
$TlGdTe_2/(TlBiTe_2)_2$	4.56	24.02	-11.3	-0.02	0.141

We then study the electronic structure of the $TlGdTe_2/(TlBiTe_2)_n$ superlattices, as previously assuming the NCAFM configuration. In Figure 3b,e, it is seen that, as compared to pure $TlGdTe_2$, the superlattices have a direct band gap (located in the A-point) and the gap size is much smaller (cf. data in Tables 1 and 2). At that, the gap of the $n = 2$ system (141 meV), having a higher Bi content, is larger than that of $n = 1$ (86 meV). The latter fact, along with the direct character of the band gap, points towards band gap inversion due to SOC, which is enhanced due to the presence of Bi. To confirm the band gap inversion we have calculated its value as a function of the SOC strength, λ. The results, presented in Figure 3c,f, show that at $\lambda/\lambda_0 \approx 0.91$ ($\lambda/\lambda_0 \approx 0.84$) the gap of the $n = 1$ ($n = 2$) system is closed, while at other values of λ/λ_0 it is non-zero, meaning that at $\lambda = \lambda_0$ it is indeed inverted around the A-point, which indicates a potential MTI state of both $TlGdTe_2/(TlBiTe_2)_n$.

Since, similarly to pure $TlGdZ_2$, we do not know the exact magnetic ground state of $TlGdTe_2/(TlBiTe_2)_n$ because of the coexistence of frustrated exchange interactions with dipolar contributions to magnetic anisotropy, we cannot reliably establish their topological classification. It should, however, be noted, that even for a complex magnetic structure, there may be a symmetry, which could give rise to a topological classification. For example, it has recently been found by neutron diffraction that $EuIn_2As_2$ exhibits a low-symmetry broken-helix antiferromagnetic order with two helix turn angles, which nevertheless supports a magnetic topological-crystalline axion insulator protected by the combination of a 180° rotation and time-reversal symmetry [65].

Taking advantage of relatively weak exchange interactions in $TlGdTe_2/(TlBiTe_2)_n$, it should in principle be possible to impose a ferromagnetically polarized state by applying an external magnetic field, as in the compounds of the $MnBi_2Te_4$ family [5,6,62]. In the artificial ferromagnetic state with a magnetization perpendicular to the Gd layers, the $TlGdTe_2/(TlBiTe_2)_n$ are characterized by gapped spectra (not shown) with bulk band gaps of 69 and 131 meV for $n = 1$ and 2, respectively. By varying the SOC constant λ we find that the band gaps are inverted, too. Moreover, the $\mathbb{Z}_4$ invariant calculations show that both systems are axion insulators ($\mathbb{Z}_4 = 2$), having the quantized topological magnetoelectric response in the bulk and chiral hinge modes [7,96]. Finally, the calculated $\mathbb{Z}_2$ invariant shows that in the paramagnetic state these systems are time-reversal symmetric strong 3D TIs.

To further illustrate the topologically non-trivial character of our superlattices, in Figure 4 we show the surface electronic structure of $TlGdTe_2/(TlBiTe_2)_1$ in the paramagnetic (PM) and ferromagnetic (FM) states. In the PM state, a linearly dispersing gapless surface state is clearly seen within the fundamental bulk band gap (Figure 4a), as expected for the time-reversal symmetric strong 3D TI. In contrast, when the system is driven in the FM state (which can be achieved by the out-of-plane external magnetic field), the Dirac point splits, consistently with what has been predicted for some compounds of the $(Mn(Bi,Sb)_2Te_4) \cdot n((Bi,Sb)_2Te_3)$ family in the FM state [55,104–106].

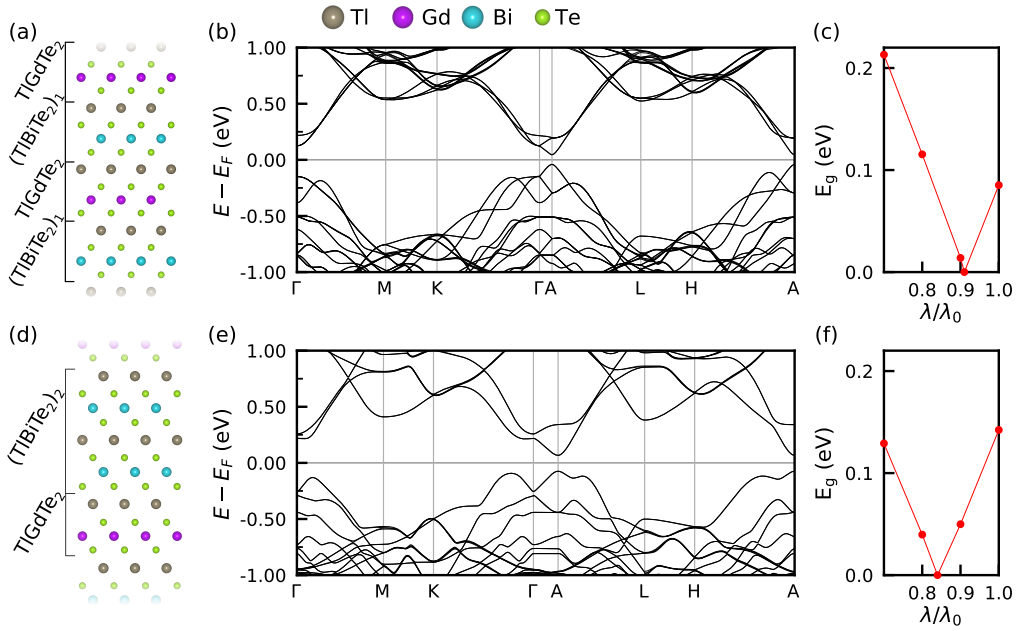

Figure 3. (**a**,**d**) Crystal structures of the $TlGdTe_2/(TlBiTe_2)_n$ superlattices for $n = 1$ (**a**) and $n = 2$ (**d**). (**b**,**e**) Bulk electronic structure of the $TlGdTe_2/(TlBiTe_2)_n$ superlattices for $n = 1$ (**b**) and $n = 2$ (**e**). Note that the number of bands is larger for the $n = 1$ system due to a larger number of the atoms in the hexagonal unit cell: 24 for $n = 1$ vs. 12 for $n = 2$. This is because the ABCABC stacking dictates that the number of atoms in the hexagonal cell is divisible by three. (**c**,**f**) Evolution of the bulk gap size with the change of the SOC constant λ from its natural strength λ_0 to about $0.7\lambda_0$. The NCAFM spin alignment in the Gd layers is assumed in the calculations.

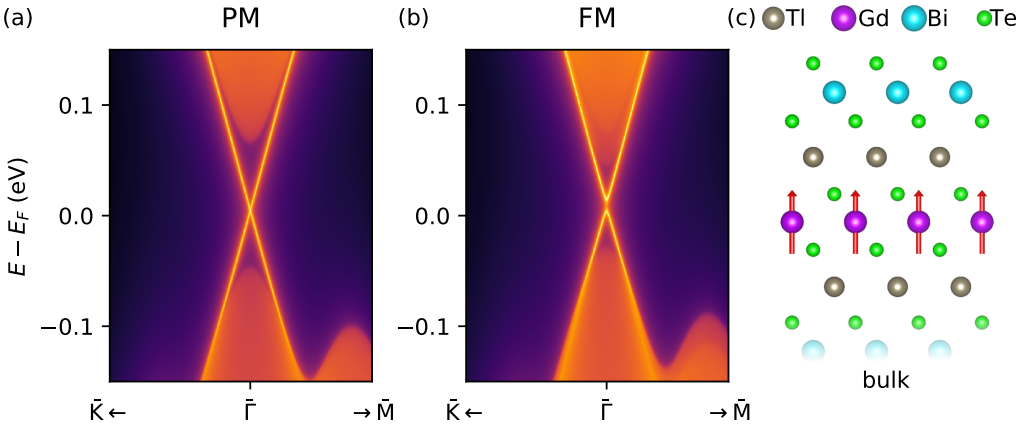

Figure 4. Surface electronic structure of $TlGdTe_2/(TlBiTe_2)_1$, calculated for the PM state (**a**) and FM state (**b**) for one the Te termination shown in (**c**). The regions with a continuous spectrum correspond to the bulk projected states.

Finally, we would like to discuss the similarities and differences between the here discussed MTI superlattices $TlGdTe_2/(TlBiTe_2)_n$ and intrinsic MTIs of the $(MnBi_2Te_4)\cdot n(Bi_2Te_3)$ and $(MnSb_2Te_4)\cdot n(Sb_2Te_3)$ families. Pretty much as the latter systems, composed of the building blocks of the magnetic $(Mn(Bi,Sb)_2Te_4)$ and nonmagnetic $((Bi,Sb)_2Te_3)$ compounds, our superlattices are made of two stoichiometric systems, too. However, while $(Mn(Bi,Sb)_2Te_4)\cdot n((Bi,Sb)_2Te_3)$ are compounds themselves, $TlGdTe_2/(TlBiTe_2)_n$ can hardly be considered as such. Indeed, $(Mn(Bi,Sb)_2Te_4)\cdot n((Bi,Sb)_2Te_3)$ can be grown in the bulk single crystal form, while applying the bulk growth strategy to the $Tl(Gd,Bi)Z_2$ system would, most likely, result in a disordered $TlGd_xBi_{1-x}Z_2$ solid solution (found to be paramagnetic down to 2 K at $x = 0.1$) [107]. In this sense, $TlGdTe_2/(TlBiTe_2)_n$ are somewhat similar to

delta-doped systems, such as digital magnetic alloys [108], representing transition metal monolayers embedded in a matrix of semiconductor material, studied previously in the field of diluted magnetic semiconductors. We propose that $TlGdTe_2/(TlBiTe_2)_n$ can be synthesized using layer-by-layer growth techniques, such as molecular beam epitaxy or atomic layer deposition, that have proven successful for growing layered van der Waals and non-van der Waals materials, complex heterostructures and superlattices [32,56,109–111].

4. Conclusions

In summary, using ab initio and tight-binding calculations we have studied magnetism and electronic structure of the $TlGdZ_2$ (Z = Se, Te) compounds as well as $TlGdTe_2/(TlBiTe_2)_n$ superlattices. Our results suggest a complex magnetic ground state in all these systems, which is due to the combination of the antiferromagnetic exchange interaction within Gd layers (resolving itself into the non-collinear spin structure), the fcc-type layer stacking, and the presence of the interlayer exchange coupling. As far as the electronic structure is concerned, $TlGdZ_2$ appear to be topologically-trivial semiconductors. However, a magnetic topological insulator state can be induced by constructing superlattices of $TlGdZ_2$ with isostructural Tl-based non-magnetic TIs. In this way, we predict that $TlGdTe_2/(TlBiTe_2)_n$ potentially hosts a magnetic topological insulator state both intrinsically and under an external magnetic field. Our study not only suggests a new approach for achieving magnetic topological states of matter, but also uncovers a new large family of the $TlREZ_2/(TlXZ_2)_n$ superlattices (RE = Pr, Nd, Sm, Gd, Tb, Dy, Ho, Er, and Tm; X = Bi, Sb; Z = S, Se, Te) with tunable magnetic, electronic and topological properties.

Supplementary Materials: The following are available online at https://www.mdpi.com/article/10.3390/nano13010038/s1, Figure S1: Comparison of the bulk electronic structures of $TlBiTe_2$ and $TlGdTe_2$.

Author Contributions: Data curation, A.Yu.V., E.K.P., I.V.S. and Yu.M.K.; Investigation, A.Yu.V., E.K.P., M.B., I.V.S. and Yu.M.K.; Supervision, M.M.O. and E.V.C.; Writing—original draft, M.M.O. and A.Yu.V.; Writing—review and editing, A.Yu.V., E.K.P., M.B., I.V.S., Yu.M.K., M.M.O. and E.V.C. All authors have read and agreed to the published version of the manuscript.

Funding: M.M.O. and M.B. acknowledge the support by Spanish Ministerio de Ciencia e Innovación (Grant No. PID2019-103910GB-I00) and the University of the Basque Country (Grant no. IT1527-22). A.Yu.V. and E.K.P. acknowledge support from the Ministry of Education and Science of the Russian Federation within State Task No. FSWM-2020-0033 (in the part of bulk and surface electronic structure calculations). E.V.C. acknowledges support from Saint Petersburg State University (Grant ID No. 90383050). Yu.M.K. acknowledges support from the Government research assignment for ISPMS SB RAS, project FWRW-2022-0001 (in the part of the topological classification of bulk band structure).

Data Availability Statement: Not applicable.

Acknowledgments: The authors thank S.V. Eremeev for stimulating discussions. Calculations were performed at the Research Park of Saint-Petersburg State University Computing Center (http://www.cc.spbu.ru/, accessed on 20 November 2022).

Conflicts of Interest: The authors declare no conflict of interest.

Abbreviations

The following abbreviations are used in this manuscript:

MTI	Magnetic topological insulator
FM	Ferromagnetic
AFM	Antiferromagnetic
NCAFM	Noncollinear antiferromagnetic
QAHE	quantum anomalous Hall effect
TME	Topological magnetoelectric effect
DFT	Density functional theory
SOC	Spin-orbit coupling

References

1. Tokura, Y.; Yasuda, K.; Tsukazaki, A. Magnetic topological insulators. *Nat. Rev. Phys.* **2019**, *1*, 126–143. [CrossRef]
2. Otrokov, M.M.; Klimovskikh, I.I.; Bentmann, H.; Estyunin, D.; Zeugner, A.; Aliev, Z.S.; Gaß, S.; Wolter, A.U.B.; Koroleva, A.V.; Shikin, A.M.; et al. Prediction and observation of an antiferromagnetic topological insulator. *Nature* **2019**, *576*, 416–422. [CrossRef] [PubMed]
3. Rienks, E.; Wimmer, S.; Sánchez-Barriga, J.; Caha, O.; Mandal, P.; Ružička, J.; Ney, A.; Steiner, H.; Volobuev, V.; Groiss, H.; et al. Large magnetic gap at the Dirac point in $Bi_2Te_3/MnBi_2Te_4$ heterostructures. *Nature* **2019**, *576*, 423–428. [CrossRef] [PubMed]
4. Zhao, Y.F.; Zhang, R.; Mei, R.; Zhou, L.J.; Yi, H.; Zhang, Y.Q.; Yu, J.; Xiao, R.; Wang, K.; Samarth, N.; et al. Tuning the Chern number in quantum anomalous Hall insulators. *Nature* **2020**, *588*, 419–423. [CrossRef] [PubMed]
5. Liu, C.; Wang, Y.; Li, H.; Wu, Y.; Li, Y.; Li, J.; He, K.; Xu, Y.; Zhang, J.; Wang, Y. Robust axion insulator and Chern insulator phases in a two-dimensional antiferromagnetic topological insulator. *Nat. Mater.* **2020**, *19*, 522–527. [CrossRef] [PubMed]
6. Deng, Y.; Yu, Y.; Shi, M.Z.; Guo, Z.; Xu, Z.; Wang, J.; Chen, X.H.; Zhang, Y. Quantum anomalous Hall effect in intrinsic magnetic topological insulator $MnBi_2Te_4$. *Science* **2020**, *367*, 895–900. [CrossRef]
7. Xu, Y.; Elcoro, L.; Song, Z.D.; Wieder, B.J.; Vergniory, M.; Regnault, N.; Chen, Y.; Felser, C.; Bernevig, B.A. High-throughput calculations of magnetic topological materials. *Nature* **2020**, *586*, 702–707. [CrossRef]
8. Deng, H.; Chen, Z.; Wołoś, A.; Konczykowski, M.; Sobczak, K.; Sitnicka, J.; Fedorchenko, I.V.; Borysiuk, J.; Heider, T.; Pluciński, L.; et al. High-temperature quantum anomalous Hall regime in a $MnBi_2Te_4/Bi_2Te_3$ superlattice. *Nat. Phys.* **2020**, *17*, 36–42. [CrossRef]
9. Gao, A.; Liu, Y.F.; Hu, C.; Qiu, J.X.; Tzschaschel, C.; Ghosh, B.; Ho, S.C.; Bérubé, D.; Chen, R.; Sun, H.; et al. Layer Hall effect in a 2D topological axion antiferromagnet. *Nature* **2021**, *595*, 521–525. [CrossRef]
10. Zhang, X.; Zhang, S.C. Chiral interconnects based on topological insulators. *Proc. SPIE* **2012**, *8373*, 837309. [CrossRef]
11. Alam, S.; Hossain, M.S.; Aziz, A. A non-volatile cryogenic random-access memory based on the quantum anomalous Hall effect. *Sci. Rep.* **2021**, *11*, 1–9. [CrossRef] [PubMed]
12. Lian, B.; Sun, X.Q.; Vaezi, A.; Qi, X.L.; Zhang, S.C. Topological quantum computation based on chiral Majorana fermions. *Proc. Natl. Acad. Sci. USA* **2018**, *115*, 10938–10942. [CrossRef] [PubMed]
13. Grushin, A.G.; Cortijo, A. Tunable Casimir Repulsion with Three-Dimensional Topological Insulators. *Phys. Rev. Lett.* **2011**, *106*, 020403. [CrossRef] [PubMed]
14. Tajik, F.; Allameh, N.; Masoudi, A.; Palasantzas, G. Nonlinear actuation of micromechanical Casimir oscillators with topological insulator materials toward chaotic motion: Sensitivity on magnetization and dielectric properties. *Chaos Interdiscip. J. Nonlinear Sci.* **2022**, *32*, 093149. [CrossRef]
15. Qi, X.L.; Hughes, T.L.; Zhang, S.C. Topological field theory of time-reversal invariant insulators. *Phys. Rev. B* **2008**, *78*, 195424. [CrossRef]
16. Chang, C.Z.; Zhang, J.; Feng, X.; Shen, J.; Zhang, Z.; Guo, M.; Li, K.; Ou, Y.; Wei, P.; Wang, L.L.; et al. Experimental Observation of the Quantum Anomalous Hall Effect in a Magnetic Topological Insulator. *Science* **2013**, *340*, 167–170. [CrossRef]
17. Essin, A.M.; Moore, J.E.; Vanderbilt, D. Magnetoelectric Polarizability and Axion Electrodynamics in Crystalline Insulators. *Phys. Rev. Lett.* **2009**, *102*, 146805. [CrossRef]
18. Tse, W.K.; MacDonald, A.H. Giant Magneto-Optical Kerr Effect and Universal Faraday Effect in Thin-Film Topological Insulators. *Phys. Rev. Lett.* **2010**, *105*, 057401. [CrossRef]
19. Katmis, F.; Lauter, V.; Nogueira, F.S.; Assaf, B.A.; Jamer, M.E.; Wei, P.; Satpati, B.; Freeland, J.W.; Eremin, I.; Heiman, D.; et al. A high-temperature ferromagnetic topological insulating phase by proximity coupling. *Nature* **2016**, *533*, 513–516. [CrossRef]
20. Bhattacharyya, S.; Akhgar, G.; Gebert, M.; Karel, J.; Edmonds, M.T.; Fuhrer, M.S. Recent Progress in Proximity Coupling of Magnetism to Topological Insulators. *Adv. Mater.* **2021**, *33*, 2007795. [CrossRef]
21. Mogi, M.; Yoshimi, R.; Tsukazaki, A.; Yasuda, K.; Kozuka, Y.; Takahashi, K.S.; Kawasaki, M.; Tokura, Y. Magnetic modulation doping in topological insulators toward higher-temperature quantum anomalous Hall effect. *Appl. Phys. Lett.* **2015**, *107*. [CrossRef]
22. Watanabe, R.; Yoshimi, R.; Kawamura, M.; Mogi, M.; Tsukazaki, A.; Yu, X.; Nakajima, K.; Takahashi, K.S.; Kawasaki, M.; Tokura, Y. Quantum anomalous Hall effect driven by magnetic proximity coupling in all-telluride based heterostructure. *Appl. Phys. Lett.* **2019**, *115*, 102403. [CrossRef]
23. Okada, K.N.; Takahashi, Y.; Mogi, M.; Yoshimi, R.; Tsukazaki, A.; Takahashi, K.S.; Ogawa, N.; Kawasaki, M.; Tokura, Y. Terahertz spectroscopy on Faraday and Kerr rotations in a quantum anomalous Hall state. *Nat. Commun.* **2016**, *7*, 12245. [CrossRef] [PubMed]
24. Fijalkowski, K.M.; Liu, N.; Hartl, M.; Winnerlein, M.; Mandal, P.; Coschizza, A.; Fothergill, A.; Grauer, S.; Schreyeck, S.; Brunner, K.; et al. Any axion insulator must be a bulk three-dimensional topological insulator. *Phys. Rev. B* **2021**, *103*, 235111. [CrossRef]
25. Mogi, M.; Okamura, Y.; Kawamura, M.; Yoshimi, R.; Yasuda, K.; Tsukazaki, A.; Takahashi, K.; Morimoto, T.; Nagaosa, N.; Kawasaki, M.; et al. Experimental signature of the parity anomaly in a semi-magnetic topological insulator. *Nat. Phys.* **2022**, *18*, 390–394. [CrossRef]

26. Lee, I.; Kim, C.K.; Lee, J.; Billinge, S.J.L.; Zhong, R.; Schneeloch, J.A.; Liu, T.; Valla, T.; Tranquada, J.M.; Gu, G.; et al. Imaging Dirac-mass disorder from magnetic dopant atoms in the ferromagnetic topological insulator $Cr_x(Bi_{0.1}Sb_{0.9})_{2-x}Te_3$. *Proc. Natl. Acad. Sci. USA* **2015**, *112*, 1316–1321. [CrossRef]
27. Lachman, E.O.; Young, A.F.; Richardella, A.; Cuppens, J.; Naren, H.; Anahory, Y.; Meltzer, A.Y.; Kandala, A.; Kempinger, S.; Myasoedov, Y.; et al. Visualization of superparamagnetic dynamics in magnetic topological insulators. *Sci. Adv.* **2015**, *1*, e1500740. [CrossRef]
28. Krieger, J.A.; Chang, C.Z.; Husanu, M.A.; Sostina, D.; Ernst, A.; Otrokov, M.M.; Prokscha, T.; Schmitt, T.; Suter, A.; Vergniory, M.G.; et al. Spectroscopic perspective on the interplay between electronic and magnetic properties of magnetically doped topological insulators. *Phys. Rev. B* **2017**, *96*, 184402. [CrossRef]
29. Otrokov, M.M.; Menshchikova, T.V.; Vergniory, M.G.; Rusinov, I.P.; Vyazovskaya, A.Y.; Koroteev, Y.M.; Bihlmayer, G.; Ernst, A.; Echenique, P.M.; Arnau, A.; et al. Highly-ordered wide bandgap materials for quantized anomalous Hall and magnetoelectric effects. *2D Mater.* **2017**, *4*, 025082. [CrossRef]
30. Otrokov, M.M.; Menshchikova, T.V.; Rusinov, I.P.; Vergniory, M.G.; Kuznetsov, V.M.; Chulkov, E.V. Magnetic extension as an efficient method for realizing the quantum anomalous Hall state in topological insulators. *JETP Lett.* **2017**, *105*, 297–302. [CrossRef]
31. Eremeev, S.V.; Otrokov, M.M.; Chulkov, E.V. Competing rhombohedral and monoclinic crystal structures in $MnPn_2Ch_4$ compounds: An ab initio study. *J. Alloys Compd.* **2017**, *709*, 172–178. [CrossRef]
32. Hirahara, T.; Eremeev, S.V.; Shirasawa, T.; Okuyama, Y.; Kubo, T.; Nakanishi, R.; Akiyama, R.; Takayama, A.; Hajiri, T.; Ideta, S.; et al. Large-gap magnetic topological heterostructure formed by subsurface incorporation of a ferromagnetic layer. *Nano Lett.* **2017**, *17*, 3493–3500. [CrossRef] [PubMed]
33. Hagmann, J.A.; Li, X.; Chowdhury, S.; Dong, S.N.; Rouvimov, S.; Pookpanratana, S.J.; Yu, K.M.; Orlova, T.A.; Bolin, T.B.; Segre, C.U.; et al. Molecular beam epitaxy growth and structure of self-assembled Bi_2Se_3/Bi_2MnSe_4 multilayer heterostructures. *New J. Phys.* **2017**, *19*, 085002. [CrossRef]
34. Otrokov, M.M.; Rusinov, I.P.; Blanco-Rey, M.; Hoffmann, M.; Vyazovskaya, A.Y.; Eremeev, S.V.; Ernst, A.; Echenique, P.M.; Arnau, A.; Chulkov, E.V. Unique Thickness-Dependent Properties of the van der Waals Interlayer Antiferromagnet $MnBi_2Te_4$ Films. *Phys. Rev. Lett.* **2019**, *122*, 107202. [CrossRef] [PubMed]
35. Li, J.; Li, Y.; Du, S.; Wang, Z.; Gu, B.L.; Zhang, S.C.; He, K.; Duan, W.; Xu, Y. Intrinsic magnetic topological insulators in van der Waals layered $MnBi_2Te_4$-family materials. *Sci. Adv.* **2019**, *5*, eaaw5685. [CrossRef] [PubMed]
36. Zhang, D.; Shi, M.; Zhu, T.; Xing, D.; Zhang, H.; Wang, J. Topological Axion States in the Magnetic Insulator $MnBi_2Te_4$ with the Quantized Magnetoelectric Effect. *Phys. Rev. Lett.* **2019**, *122*, 206401. [CrossRef] [PubMed]
37. Gong, Y.; Guo, J.; Li, J.; Zhu, K.; Liao, M.; Liu, X.; Zhang, Q.; Gu, L.; Tang, L.; Feng, X.; et al. Experimental realization of an intrinsic magnetic topological insulator. *Chinese Phys. Lett.* **2019**, *36*, 076801. [CrossRef]
38. Lee, S.H.; Zhu, Y.; Wang, Y.; Miao, L.; Pillsbury, T.; Yi, H.; Kempinger, S.; Hu, J.; Heikes, C.A.; Quarterman, P.; et al. Spin scattering and noncollinear spin structure-induced intrinsic anomalous Hall effect in antiferromagnetic topological insulator $MnBi_2Te_4$. *Phys. Rev. Res.* **2019**, *1*, 012011. [CrossRef]
39. Yan, J.Q.; Zhang, Q.; Heitmann, T.; Huang, Z.; Chen, K.Y.; Cheng, J.G.; Wu, W.; Vaknin, D.; Sales, B.C.; McQueeney, R.J. Crystal growth and magnetic structure of $MnBi_2Te_4$. *Phys. Rev. Mater.* **2019**, *3*, 064202. [CrossRef]
40. Vidal, R.C.; Bentmann, H.; Peixoto, T.R.F.; Zeugner, A.; Moser, S.; Min, C.H.; Schatz, S.; Kißner, K.; Ünzelmann, M.; Fornari, C.I.; et al. Surface states and Rashba-type spin polarization in antiferromagnetic $MnBi_2Te_4$(0001). *Phys. Rev. B* **2019**, *100*, 121104. [CrossRef]
41. Chen, B.; Fei, F.; Zhang, D.; Zhang, B.; Liu, W.; Zhang, S.; Wang, P.; Wei, B.; Zhang, Y.; Zuo, Z.; et al. Intrinsic magnetic topological insulator phases in the Sb doped $MnBi_2Te_4$ bulks and thin flakes. *Nat. Commun.* **2019**, *10*, 4469. [CrossRef] [PubMed]
42. Wu, J.; Liu, F.; Sasase, M.; Ienaga, K.; Obata, Y.; Yukawa, R.; Horiba, K.; Kumigashira, H.; Okuma, S.; Inoshita, T.; et al. Natural van der Waals heterostructural single crystals with both magnetic and topological properties. *Sci. Adv.* **2019**, *5*, eaax9989. [CrossRef] [PubMed]
43. Li, B.; Yan, J.Q.; Pajerowski, D.M.; Gordon, E.; Nedić, A.M.; Sizyuk, Y.; Ke, L.; Orth, P.P.; Vaknin, D.; McQueeney, R.J. Competing Magnetic Interactions in the Antiferromagnetic Topological Insulator $MnBi_2Te_4$. *Phys. Rev. Lett.* **2020**, *124*, 167204. [CrossRef] [PubMed]
44. Hu, C.; Gordon, K.N.; Liu, P.; Liu, J.; Zhou, X.; Hao, P.; Narayan, D.; Emmanouilidou, E.; Sun, H.; Liu, Y.; et al. A van der Waals antiferromagnetic topological insulator with weak interlayer magnetic coupling. *Nat. Commun.* **2020**, *11*, 97. [CrossRef] [PubMed]
45. Klimovskikh, I.I.; Otrokov, M.M.; Estyunin, D.; Eremeev, S.V.; Filnov, S.O.; Koroleva, A.; Shevchenko, E.; Voroshnin, V.; Rusinov, I.P.; Blanco-Rey, M.; et al. Tunable 3D/2D magnetism in the $(MnBi_2Te_4)(Bi_2T_3)_m$ topological insulators family. *Npj Quantum Mater.* **2020**, *5*, 54. [CrossRef]
46. Shikin, A.M.; Estyunin, D.A.; Zaitsev, N.L.; Glazkova, D.; Klimovskikh, I.I.; Filnov, S.O.; Rybkin, A.G.; Schwier, E.F.; Kumar, S.; Kimura, A.; et al. Sample-dependent Dirac-point gap in $MnBi_2Te_4$ and its response to applied surface charge: A combined photoemission and ab initio study. *Phys. Rev. B* **2021**, *104*, 115168. [CrossRef]
47. Petrov, E.K.; Men'shov, V.N.; Rusinov, I.P.; Hoffmann, M.; Ernst, A.; Otrokov, M.M.; Dugaev, V.K.; Menshchikova, T.V.; Chulkov, E.V. Domain wall induced spin-polarized flat bands in antiferromagnetic topological insulators. *Phys. Rev. B* **2021**, *103*, 235142. [CrossRef]

48. Wang, P.; Ge, J.; Li, J.; Liu, Y.; Xu, Y.; Wang, J. Intrinsic magnetic topological insulators. *Innovation* **2021**, *2*, 100098. [CrossRef]
49. Garnica, M.; Otrokov, M.M.; Aguilar, P.C.; Klimovskikh, I.I.; Estyunin, D.; Aliev, Z.S.; Amiraslanov, I.R.; Abdullayev, N.A.; Zverev, V.N.; Babanly, M.B.; et al. Native point defects and their implications for the Dirac point gap at $MnBi_2Te_4$(0001). *Npj Quantum Mater.* **2022**, *7*, 7. [CrossRef]
50. Mong, R.S.K.; Essin, A.M.; Moore, J.E. Antiferromagnetic topological insulators. *Phys. Rev. B* **2010**, *81*, 245209. [CrossRef]
51. Aliev, Z.S.; Amiraslanov, I.R.; Nasonova, D.I.; Shevelkov, A.V.; Abdullayev, N.A.; Jahangirli, Z.A.; Orujlu, E.N.; Otrokov, M.M.; Mamedov, N.T.; Babanly, M.B.; et al. Novel ternary layered manganese bismuth tellurides of the MnTe-Bi_2Te_3 system: Synthesis and crystal structure. *J. Alloys Compd.* **2019**, *789*, 443 – 450. [CrossRef]
52. Vidal, R.C.; Zeugner, A.; Facio, J.I.; Ray, R.; Haghighi, M.H.; Wolter, A.U.; Bohorquez, L.T.C.; Caglieris, F.; Moser, S.; Figgemeier, T.; et al. Topological Electronic Structure and Intrinsic Magnetization in $MnBi_4Te_7$: A Bi_2 Te_3 Derivative with a Periodic Mn Sublattice. *Phys. Rev. X* **2019**, *9*, 041065. [CrossRef]
53. Jahangirli, Z.A.; Alizade, E.H.; Aliev, Z.S.; Otrokov, M.M.; Ismayilova, N.A.; Mammadov, S.N.; Amiraslanov, I.R.; Mamedov, N.T.; Orudjev, G.S.; Babanly, M.B.; et al. Electronic structure and dielectric function of Mn-Bi-Te layered compounds. *J. Vac. Sci. Technol. B* **2019**, *37*, 062910. [CrossRef]
54. Yan, J.Q.; Okamoto, S.; McGuire, M.A.; May, A.F.; McQueeney, R.J.; Sales, B.C. Evolution of structural, magnetic, and transport properties in $MnBi_{2-x}Sb_xTe_4$. *Phys. Rev. B* **2019**, *100*, 104409. [CrossRef]
55. Eremeev, S.V.; Rusinov, I.P.; Koroteev, Y.M.; Vyazovskaya, A.Y.; Hoffmann, M.; Echenique, P.M.; Ernst, A.; Otrokov, M.M.; Chulkov, E.V. Topological Magnetic Materials of the $(MnSb_2Te_4)\cdot(Sb_2Te_3)_n$ van der Waals Compounds Family. *J. Phys. Chem. Lett.* **2021**, *12*, 4268. [CrossRef]
56. Wimmer, S.; Sánchez-Barriga, J.; Küppers, P.; Ney, A.; Schierle, E.; Freyse, F.; Caha, O.; Michalicka, J.; Liebmann, M.; Primetzhofer, D.; et al. Mn-Rich $MnSb_2Te_4$: A Topological Insulator with Magnetic Gap Closing at High Curie Temperatures of 45–50 K. *Adv. Mater.* **2021**, *33*, 2102935. [CrossRef]
57. Li, Y.; Jiang, Y.; Zhang, J.; Liu, Z.; Yang, Z.; Wang, J. Intrinsic topological phases in $Mn_2Bi_2Te_5$ tuned by the layer magnetization. *Phys. Rev. B* **2020**, *102*, 121107(R). [CrossRef]
58. Cao, L.; Han, S.; Lv, Y.Y.; Wang, D.; Luo, Y.C.; Zhang, Y.Y.; Yao, S.H.; Zhou, J.; Chen, Y.B.; Zhang, H.; et al. Growth and characterization of the dynamical axion insulator candidate $Mn_2Bi_2Te_5$ with intrinsic antiferromagnetism. *Phys. Rev. B* **2021**, *104*, 054421. [CrossRef]
59. Eremeev, S.V.; Otrokov, M.M.; Ernst, A.; Chulkov, E.V. Magnetic ordering and topology in $Mn_2Bi_2Te_5$ and $Mn_2Sb_2Te_5$ van der Waals materials. *Phys. Rev. B* **2022**, *105*, 195105. [CrossRef]
60. Chowdhury, S.; Garrity, K.F.; Tavazza, F. Prediction of Weyl semimetal and antiferromagnetic topological insulator phases in Bi_2MnSe_4. *npj Comput. Mater.* **2019**, *5*, 33. [CrossRef]
61. Zhu, T.; Bishop, A.J.; Zhou, T.; Zhu, M.; O'Hara, D.J.; Baker, A.A.; Cheng, S.; Walko, R.C.; Repicky, J.J.; Liu, T.; et al. Synthesis, Magnetic Properties, and Electronic Structure of Magnetic Topological Insulator $MnBi_2Se_4$. *Nano Lett.* **2021**, *21*, 5083–5090. [CrossRef] [PubMed]
62. Ge, J.; Liu, Y.; Li, J.; Li, H.; Luo, T.; Wu, Y.; Xu, Y.; Wang, J. High-Chern-number and high-temperature quantum Hall effect without Landau levels. *Natl. Sci. Rev.* **2020**, *7*, 1280–1287. [CrossRef] [PubMed]
63. Xu, Y.; Song, Z.; Wang, Z.; Weng, H.; Dai, X. Higher-Order Topology of the Axion Insulator $EuIn_2As_2$. *Phys. Rev. Lett.* **2019**, *122*, 256402. [CrossRef] [PubMed]
64. Sato, T.; Wang, Z.; Takane, D.; Souma, S.; Cui, C.; Li, Y.; Nakayama, K.; Kawakami, T.; Kubota, Y.; Cacho, C.; et al. Signature of band inversion in the antiferromagnetic phase of axion insulator candidate $EuIn_2As_2$. *Phys. Rev. Res.* **2020**, *2*, 033342. [CrossRef]
65. Riberolles, S.X.M.; Trevisan, T.V.; Kuthanazhi, B.; Heitmann, T.W.; Ye, F.; Johnston, D.C.; Bud'ko, S.L.; Ryan, D.H.; Canfield, P.C.; Kreyssig, A.; et al. Magnetic crystalline-symmetry-protected axion electrodynamics and field-tunable unpinned Dirac cones in $EuIn_2As_2$. *Nat. Commun.* **2021**, *12*, 1–7. [CrossRef]
66. Eremeev, S.V.; Landolt, G.; Menshchikova, T.V.; Slomski, B.; Koroteev, Y.M.; Aliev, Z.S.; Babanly, M.B.; Henk, J.; Ernst, A.; Patthey, L.; et al. Atom-specific spin mapping and buried topological states in a homologous series of topological insulators. *Nat. Commun.* **2012**, *3*, 635. [CrossRef]
67. Kuroda, K.; Ye, M.; Kimura, A.; Eremeev, S.V.; Krasovskii, E.E.; Chulkov, E.V.; Ueda, Y.; Miyamoto, K.; Okuda, T.; Shimada, K.; et al. Experimental Realization of a Three-Dimensional Topological Insulator Phase in Ternary Chalcogenide $TlBiSe_2$. *Phys. Rev. Lett.* **2010**, *105*, 146801. [CrossRef]
68. Sato, T.; Segawa, K.; Guo, H.; Sugawara, K.; Souma, S.; Takahashi, T.; Ando, Y. Direct Evidence for the Dirac-Cone Topological Surface States in the Ternary Chalcogenide $TlBiSe_2$. *Phys. Rev. Lett.* **2010**, *105*, 136802. [CrossRef]
69. Eremeev, S.V.; Koroteev, Y.M.; Chulkov, E.V. Ternary thallium-based semimetal chalcogenides Tl-V-VI_2 as a new class of three-dimensional topological insulators. *JETP Lett.* **2010**, *91*, 594–598. [CrossRef]
70. Eremeev, S.V.; Bihlmayer, G.; Vergniory, M.; Koroteev, Y.M.; Menshchikova, T.V.; Henk, J.; Ernst, A.; Chulkov, E.V. Ab initio electronic structure of thallium-based topological insulators. *Phys. Rev. B* **2011**, *83*, 205129. [CrossRef]
71. Duczmal, M.; Pawlak, L. Magnetic and structural characterization of $TlLnSe_2$ compounds (Ln ≡ Nd to Yb). *J. Alloys Compd.* **1995**, *225*, 181–184. [CrossRef]
72. Duczmal, M.; Pawlak, L. Magnetic properties and crystal field effects in $TlLnX_2$ compounds (X = S, Se, Te). *J. Alloys Compd.* **1997**, *262*, 316–319. [CrossRef]

73. Sankar, C.R.; Bangarigadu-Sanasy, S.; Kleinke, H. Thermoelectric Properties of $TlGdQ_2$ (Q = Se, Te) and Tl_9GdTe_6. *J. Electron. Mater.* **2012**, *41*, 1662–1666. [CrossRef]
74. Imamaliyeva, S.Z.; Babanly, D.M.; Gasanly, T.M.; Tagiyev, D.B.; Babanly, M.B. Thermodynamic Properties of Tl_9GdTe_6 and $TlGdTe_2$. *Russ. J. Phys. Chem.* **2018**, *92*, 2111–2117. [CrossRef]
75. Duczmal, M.; Mosiniewicz-Szablewska, E.; Pokrzywnicki, S. Electron paramagnetic resonance of Gd^{3+} in $TlGdSe_2$. *Phys. Status Solidi A* **2003**, *196*, 321–324. [CrossRef]
76. Gautam, R.; Kumar, A.; Singh, R.P. First Principle Investigations on Electronic, Magnetic, Thermodynamic, and Transport Properties of $TlGdX_2$ (X = S, Se, Te). *Acta Phys. Pol. B* **2017**, *132*, 1371–1378.
77. Godzhaev, E.M.; Dzhafarova, G.S. Phase Relations and Properties of Phases in the $TlInSe_2$–$TlPrSe_2$ System. *Inorg. Mater.* **2003**, *39*, 6–9. [CrossRef]
78. Blöchl, P.E. Projector augmented-wave method. *Phys. Rev. B* **1994**, *50*, 17953–17979. [CrossRef] [PubMed]
79. Kresse, G.; Furthmüller, J. Efficient iterative schemes for ab initio total-energy calculations using a plane-wave basis set. *Phys. Rev. B* **1996**, *54*, 11169–11186. [CrossRef]
80. Kresse, G.; Joubert, D. From ultrasoft pseudopotentials to the projector augmented-wave method. *Phys. Rev. B* **1999**, *59*, 1758–1775. [CrossRef]
81. Perdew, J.P.; Burke, K.; Ernzerhof, M. Generalized gradient approximation made simple. *Phys. Rev. Lett.* **1996**, *77*, 3865. [CrossRef] [PubMed]
82. Koelling, D.D.; Harmon, B.N. A technique for relativistic spin-polarised calculations. *J. Phys. Solid State Phys.* **1977**, *10*, 3107. [CrossRef]
83. Anisimov, V.I.; Zaanen, J.; Andersen, O.K. Band theory and Mott insulators: Hubbard *U* instead of Stoner *I*. *Phys. Rev. B* **1991**, *44*, 943. [CrossRef] [PubMed]
84. Dudarev, S.; Botton, G.; Savrasov, S.; Humphreys, C.; Sutton, A. Electron-energy-loss spectra and the structural stability of nickel oxide: An LSDA+ U study. *Phys. Rev. B* **1998**, *57*, 1505. [CrossRef]
85. Anisimov, V.I.; Aryasetiawan, F.; Lichtenstein, A. First-principles calculations of the electronic structure and spectra of strongly correlated systems: The LDA+ U method. *J. Phys. Condens. Matter* **1997**, *9*, 767. [CrossRef]
86. Schulz, S.; Vyazovskaya, A.Y.; Poelchen, G.; Generalov, A.; Güttler, M.; Mende, M.; Danzenbächer, S.; Otrokov, M.M.; Balasubramanian, T.; Polley, C.; et al. Classical and cubic Rashba effect in the presence of in-plane $4f$ magnetism at the iridium silicide surface of the antiferromagnet $GdIr_2Si_2$. *Phys. Rev. B* **2021**, *103*, 035123. [CrossRef]
87. Wimmer, E.; Krakauer, H.; Weinert, M.; Freeman, A.J. Full-potential self-consistent linearized-augmented-plane-wave method for calculating the electronic structure of molecules and surfaces: O_2 molecule. *Phys. Rev. B* **1981**, *24*, 864. [CrossRef]
88. Shick, A.B.; Liechtenstein, A.I.; Pickett, W.E. Implementation of the LDA+ U method using the full-potential linearized augmented plane-wave basis. *Phys. Rev. B* **1999**, *60*, 10763. [CrossRef]
89. Anisimov, V.I.; Solovyev, I.V.; Korotin, M.A.; Czyżyk, M.T.; Sawatzky, G.A. Density-functional theory and NiO photoemission spectra. *Phys. Rev. B* **1993**, *48*, 16929. [CrossRef]
90. FLEUR Site. Available online: http://www.flapw.de (accessed on 20 November 2022).
91. Marzari, N.; Vanderbilt, D. Maximally Localized Generalized Wannier Functions for Composite Energy Bands. *Phys. Rev. B* **1997**, *56*, 12847. [CrossRef]
92. Mostofi, A.; Yates, J.R.; Pizzi, G.; Lee, Y.S.; Souza, I.; Vanderbilt, D.; Marzari, N. An Updated Version of wannier90: A Tool for Obtaining Maximally-Localised Wannier Functions. *Comput. Phys. Commun.* **2014**, *185*, 2309–2310. [CrossRef]
93. Sancho, M.P.L.; Sancho, J.M.L.; Sancho, J.M.L.; Rubio, J. Highly Convergent Schemes for the Calculation of Bulk and Surface Green Functions. *J. Phys. F Met. Phys.* **1985**, *15*, 851–858. [CrossRef]
94. Wu, Q.; Zhang, S.; Song, H.F.; Troyer, M.; Soluyanov, A. WannierTools : An Open-Source Software Package for Novel Topological Materials. *Comput. Phys. Commun.* **2018**, *224*, 405–416. [CrossRef]
95. Fu, L.; Kane, C.L.; Mele, E.J. Topological insulators in three dimensions. *Phys. Rev. Lett.* **2007**, *98*, 106803. [CrossRef] [PubMed]
96. Takahashi, R.; Tanaka, Y.; Murakami, S. Bulk-edge and bulk-hinge correspondence in inversion-symmetric insulators. *Phys. Rev. Res.* **2020**, *2*, 013300. [CrossRef]
97. Lee, D.H.; Joannopoulos, J.D.; Negele, J.W.; Landau, D.P. Symmetry analysis and Monte Carlo study of a frustrated antiferromagnetic planar (XY) model in two dimensions. *Phys. Rev. B* **1986**, *33*, 450–475. [CrossRef]
98. Duczmal, M.; Pawlak, L.; Pokrzywnicki, S. Magnetic Properties of Layer-Type Compounds $TlGdS_2$ and $TlGdSe_2$. *Acta Phys. Pol. A* **2000**, *5*, 839–842. [CrossRef]
99. Clark, J.K.; Pak, C.; Cao, H.; Shatruk, M. Helimagnetism in $MnBi_2Se_4$ driven by spin-frustrating interactions between antiferromagnetic chains. *Crystals* **2021**, *11*, 242. [CrossRef]
100. Sukhanov, A.; Tymoshenko, Y.; Kulbakov, A.; Cameron, A.; Kocsis, V.; Walker, H.; Ivanov, A.; Park, J.; Pomjakushin, V.; Nikitin, S.; et al. Frustration model and spin excitations in the helimagnet FeP. *Phys. Rev. B* **2022**, *105*, 134424. [CrossRef]
101. Hayashida, S.; Ishikawa, H.; Okamoto, Y.; Okubo, T.; Hiroi, Z.; Avdeev, M.; Manuel, P.; Hagihala, M.; Soda, M.; Masuda, T. Magnetic state selected by magnetic dipole interaction in the kagome antiferromagnet $NaBa_2Mn_3F_{11}$. *Phys. Rev. B* **2018**, *97*, 054411. [CrossRef]
102. Maksymenko, M.; Chandra, V.R.; Moessner, R. Classical dipoles on the kagome lattice. *Phys. Rev. B* **2015**, *91*, 184407. [CrossRef]
103. Johnston, D.C. Magnetic dipole interactions in crystals. *Phys. Rev. B* **2016**, *93*, 014421. [CrossRef]

104. Zhang, R.X.; Wu, F.; Das Sarma, S. Möbius Insulator and Higher-Order Topology in $MnBi_{2n}Te_{3n+1}$. *Phys. Rev. Lett.* **2020**, *124*, 136407. [CrossRef] [PubMed]
105. Hu, C.; Ding, L.; Gordon, K.N.; Ghosh, B.; Tien, H.J.; Li, H.; Linn, A.G.; Lien, S.W.; Huang, C.Y.; Mackey, S.; et al. Realization of an intrinsic ferromagnetic topological state in $MnBi_8Te_{13}$. *Sci. Adv.* **2020**, *6*, eaba4275. [CrossRef] [PubMed]
106. Jo, N.H.; Wang, L.L.; Slager, R.J.; Yan, J.; Wu, Y.; Lee, K.; Schrunk, B.; Vishwanath, A.; Kaminski, A. Intrinsic axion insulating behavior in antiferromagnetic $MnBi_6Te_{10}$. *Phys. Rev. B* **2020**, *102*, 045130. [CrossRef]
107. Filnov, S.O.; Klimovskikh, I.I.; Estyunin, D.A.; Fedorov, A.V.; Voroshnin, V.Y.; Koroleva, A.V.; Rybkin, A.G.; Shevchenko, E.V.; Aliev, Z.S.; Babanly, M.B.; et al. Probe-dependent Dirac-point gap in the gadolinium-doped thallium-based topological insulator $TlBi_{0.9}Gd_{0.1}Se_2$. *Phys. Rev. B* **2020**, *102*, 085149. [CrossRef]
108. Otrokov, M.M.; Ernst, A.; Tugushev, V.V.; Ostanin, S.; Buczek, P.; Sandratskii, L.M.; Fischer, G.; Hergert, W.; Mertig, I.; Kuznetsov, V.M.; et al. Ab initio study of the magnetic ordering in Si/Mn digital alloys. *Phys. Rev. B* **2011**, *84*, 144431. [CrossRef]
109. Hirahara, T.; Otrokov, M.M.; Sasaki, T.; Sumida, K.; Tomohiro, Y.; Kusaka, S.; Okuyama, Y.; Ichinokura, S.; Kobayashi, M.; Takeda, Y.; et al. Fabrication of a novel magnetic topological heterostructure and temperature evolution of its massive Dirac cone. *Nat. Commun.* **2020**, *11*, 4821. [CrossRef]
110. Su, S.H.; Chang, J.T.; Chuang, P.Y.; Tsai, M.C.; Peng, Y.W.; Lee, M.K.; Cheng, C.M.; Huang, J.C.A. Epitaxial Growth and Structural Characterizations of $MnBi_2Te_4$ Thin Films in Nanoscale. *Nanomaterials* **2021**, *11*, 3322. [CrossRef]
111. Johnson, R.W.; Hultqvist, A.; Bent, S.F. A brief review of atomic layer deposition: From fundamentals to applications. *Mater. Today* **2014**, *17*, 236–246. [CrossRef]